APPLIED SCIENCES AND ENGINEERING

Reprogrammable shape morphing of magnetic soft machines

Yunus Alapan[1]*, Alp C. Karacakol[1,2]*, Seyda N. Guzelhan[1], Irem Isik[1], Metin Sitti[1,3,4]†

Copyright © 2020 The Authors, some rights reserved; exclusive licensee American Association for the Advancement of Science. No claim to original U.S. Government Works. Distributed under a Creative Commons Attribution NonCommercial License 4.0 (CC BY-NC).

Shape-morphing magnetic soft machines are highly desirable for diverse applications in minimally invasive medicine, wearable devices, and soft robotics. Despite recent progress, current magnetic programming approaches are inherently coupled to sequential fabrication processes, preventing reprogrammability and high-throughput programming. Here, we report a high-throughput magnetic programming strategy based on heating magnetic soft materials above the Curie temperature of the embedded ferromagnetic particles and reorienting their magnetic domains by applying magnetic fields during cooling. We demonstrate discrete, three-dimensional, and reprogrammable magnetization with high spatial resolution (~38 μm). Using the reprogrammable magnetization capability, reconfigurable mechanical behavior of an auxetic metamaterial structure, tunable locomotion of a surface-walking soft robot, and adaptive grasping of a soft gripper are shown. Our approach further enables high-throughput magnetic programming (up to 10 samples/min) via contact transfer. Heat-assisted magnetic programming strategy described here establishes a rich design space and mass-manufacturing capability for development of multiscale and reprogrammable soft machines.

INTRODUCTION

Shape-morphing materials that can be actuated via external stimuli, such as light, temperature, humidity, pH, and acoustic, electrical and magnetic fields, hold great importance for future applications in minimally invasive medicine (*1*–*3*), implantable and wearable devices (*4*, *5*), soft robotics (*6*–*9*), and micromachines (*10*–*12*). Magnetically responsive soft materials with programmable shape deformation are particularly desirable for fast, reversible, and complex morphing of soft machines (*5*, *6*, *10*, *11*, *13*, *14*). Magneto-active properties of these soft machines stem from magnetic micro/nanoparticles distributed within a soft polymer matrix. Applied magnetic fields generate torque on magnetic soft materials until the magnetization direction of all domains is aligned with the field direction (*15*–*17*). Therefore, creating a spatial distribution of magnetization directions in a magnetic soft machine enables programmable shape deformation under magnetic fields (*6*, *11*, *13*, *18*–*20*).

Initial approaches for magnetic programming of soft machines rely on template-assisted magnetization. A magnetic soft material is deformed into a predetermined shape under a saturating uniform magnetic field, resulting in reorientation of the magnetic domains in the field direction. When unfolded, the magnetic soft material exhibits spatially varying magnetization directions (*6*, *18*). Although template-assisted magnetic programming allows facile encoding of deformation instructions, creating discrete three-dimensional (3D) magnetization profiles at small scales is challenging due to intricate template geometries and handling. Recently, other magnetic programming approaches are introduced for encoding discrete 3D magnetization profiles in small-scale soft machines based on physical alignment and fixing of the magnetic particles during curing via lithographic or 3D printing techniques (*7*, *13*, *21*). However, in these approaches, magnetic programming is inherently coupled to the fabrication process, resulting in a permanent magnetization profile, which prevents reprogramming once fabricated (*7*, *13*, *21*). Furthermore, sequential magnetization and fabrication processes associated with these approaches limit high-throughput magnetic programming.

Here, we introduce a versatile strategy for encoding reprogrammable shape-morphing instructions into magnetic soft machines in a high-throughput fashion. Our approach is enabled by heat-assisted magnetic programming of soft materials by heating above the Curie temperature of the ferromagnetic particles and reorienting their magnetic domains with external magnetic fields during cooling (Fig. 1A). By heat-assisted magnetization, shape-changing instructions in 3D can be encoded discretely and reprogrammed on demand with high resolution (~38 μm). Taking advantage of magnetic reprogrammability, reconfigurable mechanical behavior of an auxetic metamaterial structure, tunable locomotion patterns of a quadrupedal soft robot, and adaptive grasping behavior of a soft gripper are demonstrated. Heat-assisted magnetic programming further enables high-throughput magnetic programming via contact transfer of distributed magnetization profiles from a magnetic master (~10 samples/min using a single master). The magnetic (re)programming approach described here is a versatile and powerful tool for the development of next-generation small-scale magnetic soft machines with unprecedented shape-morphing capabilities.

RESULTS

Our magnetic soft machines are composed of chromium dioxide (CrO_2) microparticles with an average diameter of 10 μm embedded in a polydimethylsiloxane (PDMS) elastomer. CrO_2 is a ferromagnetic material (fig. S1A), which has a Curie temperature of 118°C, enabling heat-assisted magnetic (re)programming within the operation temperature of most elastomers (*22*). The CrO_2/PDMS magnetic soft elastomer composite sheets are prepared by curing the CrO_2 particles and PDMS mixture in molds of different thicknesses, resulting in magneto-elastic films in a thickness range of 25 to 200 μm (fig. S2A). A collimated near-infrared (NIR) laser with tunable power is used for heating the magnetic soft elastomers locally and precisely

[1]Physical Intelligence Department, Max Planck Institute for Intelligent Systems, 70569 Stuttgart, Germany. [2]Department of Mechanical Engineering, Carnegie Mellon University, Pittsburgh, PA 15213, USA. [3]School of Medicine and School of Engineering, Koç University, 34450 Istanbul, Turkey. [4]Institute for Biomedical Engineering, ETH Zurich, 8092 Zurich, Switzerland.
*These authors contributed equally to this work as co-first authors.
†Corresponding author. Email: sitti@is.mpg.de

Downloaded from http://advances.sciencemag.org/ on November 19, 2020

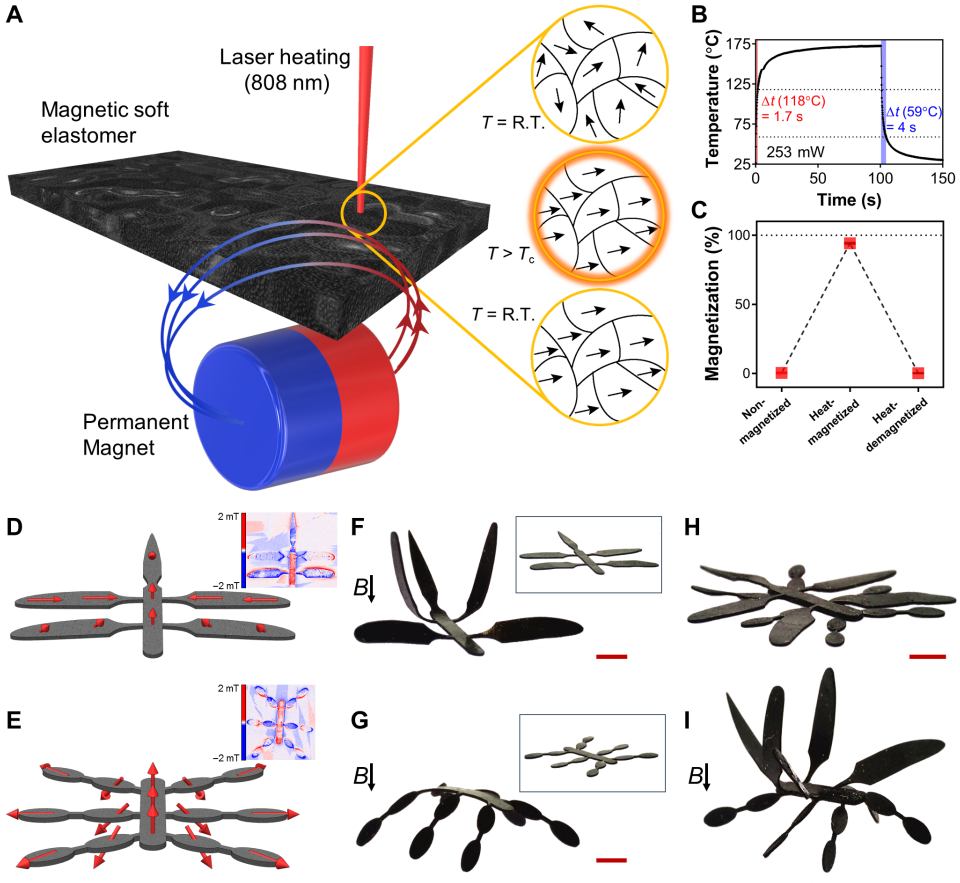


Fig. 1. Heat-assisted 3D magnetic programming of magnetic soft machines. (**A**) A magnetic soft elastomer, composed of magnetic CrO_2 particles embedded in PDMS, is locally heated above the Curie temperature of the particles via a laser. Above the Curie temperature, the particles lose their permanent magnetization, and their magnetization direction is reoriented by applying an external magnetic field during cooling. R.T., room temperature. (**B**) The magnetic soft elastomer is heated above the Curie temperature of the CrO_2 particles (118°C) in 1.7 s and cooled down to half of this temperature in 4 s. (**C**) The magnetic soft elastomer is magnetized with 90% efficiency by heat-assisted magnetization and demagnetized by only heating above the Curie temperature without any external magnetic field. Error bars represent the SD of the mean. (**D** to **G**) Examples of the magnetic soft elastomer cut into the shapes of a body with a tail and wings (D) and a six-legged body (E) with corresponding magnetization directions (indicated by red arrows) and out-of-plane magnetic flux profile measurements. Color bars indicate magnetic flux density strength. (**F** and **G**) Upon magnetic actuation, individual parts underwent shape change in accordance with their programmed magnetization directions. Scale bars, 2 mm. Insets show the initial shape of the structures in the absence of magnetic fields. (**H** and **I**) Bodies with wings and legs are stacked to generate a 3D hierarchical dragonfly structure upon magnetic actuation. Scale bar, 2 mm. Actuation of the structures is performed by applying magnetic fields of 60 mT in the directions indicated with the black arrows.

with controlled temperature, heating-cooling duration, and heated spot size (Fig. 1B and fig. S3). The shortest heating-cooling cycle in a 1.3-mm-diameter heated spot is achieved in 5.7 s (Fig. 1B). The laser-heated magnetic soft elastomer spots are magnetized via external magnetic fields exceeding 15 mT, resulting in more than 90% magnetization efficiency in comparison to maximum achievable magnetization under a 1.8-T magnetic field (fig. S1B). These high magnetization efficiencies indicate almost complete reorientation of magnetic domains in the desired direction while minimizing undesired magnetization in other directions. The same materials can be then demagnetized locally or fully by heating again above the Curie temperature of CrO_2 particles in the absence of a magnetic field (Fig. 1C and fig. S1C). Momentary heating has a limited effect on the mechanical properties of the magnetic soft elastomers (fig. S2, B to F), since the applied temperatures are well within the curing and operation temperature range of PDMS (*23*), enabling noninvasive magnetic programming and reprogramming.

To illustrate heat-assisted magnetic programming of CrO_2 particle–embedded soft machines, we present planar magnetic soft elastomer films cut into shapes of a body with a tail and wings and a six-legged body (Fig. 1, D to H). Bodies and extremities are discretely magnetized in varying 3D directions (Fig. 1, D and E), and magnetization directions are validated by measuring out-of-plane components of their magnetic flux density as shown in insets of Fig. 1, D and E. Upon application of a magnetic field of 60 mT perpendicular to the plane, magnetic torques on components with different magnetization directions try to align them in the direction of the external field, resulting in 3D deformations of the structures (Fig. 1, F and G, and movie S1). Furthermore, multicomponent 3D structures can be formed by stacking individual components, as shown in Fig. 1H. The bodies with legs and wings are stacked to form a multicomponent 3D "dragonfly" structure upon magnetic actuation (Fig. 1I and movie S1).

In Fig. 2, we present a set of structures with varying 3D magnetization profiles that can transform into complex 3D structures

Downloaded from http://advances.sciencemag.org/ on November 19, 2020

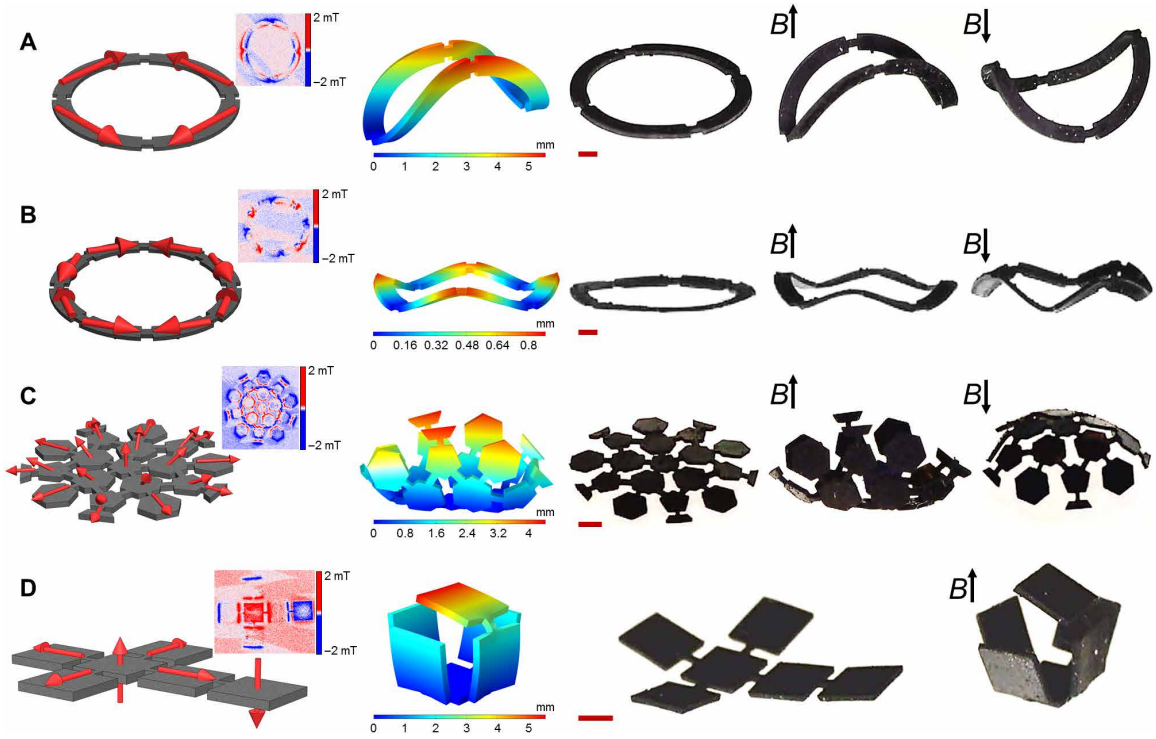


Fig. 2. Discrete and 3D magnetization of magnetic soft structures. (**A** to **D**) Distributed 3D magnetizations, out-of-plane magnetic flux density profile measurements, finite element simulations, and experimental shape changes upon magnetic actuation of a four-segment ring (A), eight-segment ring (B), a half-sphere (C), and a cube structure (D). Scale bars, 1 mm. Actuation was performed by applying a magnetic field of 60 mT in the directions indicated with the black arrows.

under magnetic fields (movie S1). We develop a computational model, taking magnetization directions, external magnetic fields, and mechanical deformations into account, to predict the complex 3D shape transformations with the designed magnetization profiles (Fig. 2). While a ring structure with a four-segmented alternating magnetization profile generates a vertically rising structure upon magnetic actuation (Fig. 2A), a ring of the same size with an eight-segmented alternating magnetization profile results in undulating edges (Fig. 2B). A 3D half-sphere structure is formed by radially symmetric magnetization of a planar structure composed of hexagonal and pentagonal units connected through hinges (Fig. 2C). Moreover, stacking two of these structures with complementing magnetization profiles enables the formation of a closed 3D sphere, which can also be rolled on a planar surface by applying rotating magnetic fields (fig. S4 and movie S1). The formation of closed structures can be also realized by complementary 3D magnetization, thus deformation, of connected segments. Planar segments connected via hinges are magnetized both in-plane and out-of-plane to form a closed cube under a magnetic field of 60 mT (Fig. 2D and movie S1).

In situ magnetic reprogramming of soft machines is crucial for their optimization, multifunctional operation, and adaptation to dynamic environments. Heat-assisted magnetization strategy allows facile magnetic reprogramming of soft structures on demand. In Fig. 3A, we present a "stickman" structure with a 3D magnetization profile encoded in the body, shoulders, arms, and head, which undergoes a 3D complex shape transformation upon magnetic actuation (movie S2). When the magnetization profile of the stickman structure is reprogrammed, bending of its head and arms can be reconfigured, as shown in Fig. 3B and C and movie S2. Local reprogramming of internal material behavior can also enable the design and optimization of advanced active metamaterials. In Fig. 3D, we present an auxetic mechanical metamaterial structure composed of eight units. Magnetic programming of the units as shown in Fig. 3E results in expansion and compression of the whole structure both in length and width at the same time, thus displaying a negative Poisson's ratio, depending on the magnetic actuation direction (Fig. 3, F and G, and movie S2). Using the heat-assisted magnetic reprogramming approach, the magnetization profile of individual units, thus their mechanical behavior, can be reprogrammed (fig. S5, A to G). Reprogramming of multiple units in the middle section of the structure results in an expansion in width with minimal change in length, independent of the magnetic actuation direction (Fig. 3, H to J). To further highlight the importance of facile reprogramming, we demonstrate a quadrupedal flexible robot with a specific magnetization direction assigned for each leg (Fig. 3, K to P; fig. S5, H to J; and movie S2). The asymmetric magnetization of legs at two lateral sides generates larger deformation of the right legs and generates a circular trajectory upon magnetic actuation (Fig. 3, K to M). Reprogramming magnetization profiles of the soft robot with bilateral and fore-and-aft symmetries results in laterally symmetric deformations of the legs and generate straight trajectories upon magnetic actuation (Fig. 3, N to P, and movie S2). These results show that remote and noninvasive reprogramming can be used for experimental optimization of the material behavior, such as in mechanical and acoustic metamaterials, and tuning the locomotion performance and characteristics of soft robots.

Heat-assisted magnetization can also be extended for programming 2D structures arranged in 3D configurations. In Fig. 4A, we

Downloaded from http://advances.sciencemag.org/ on November 19, 2020

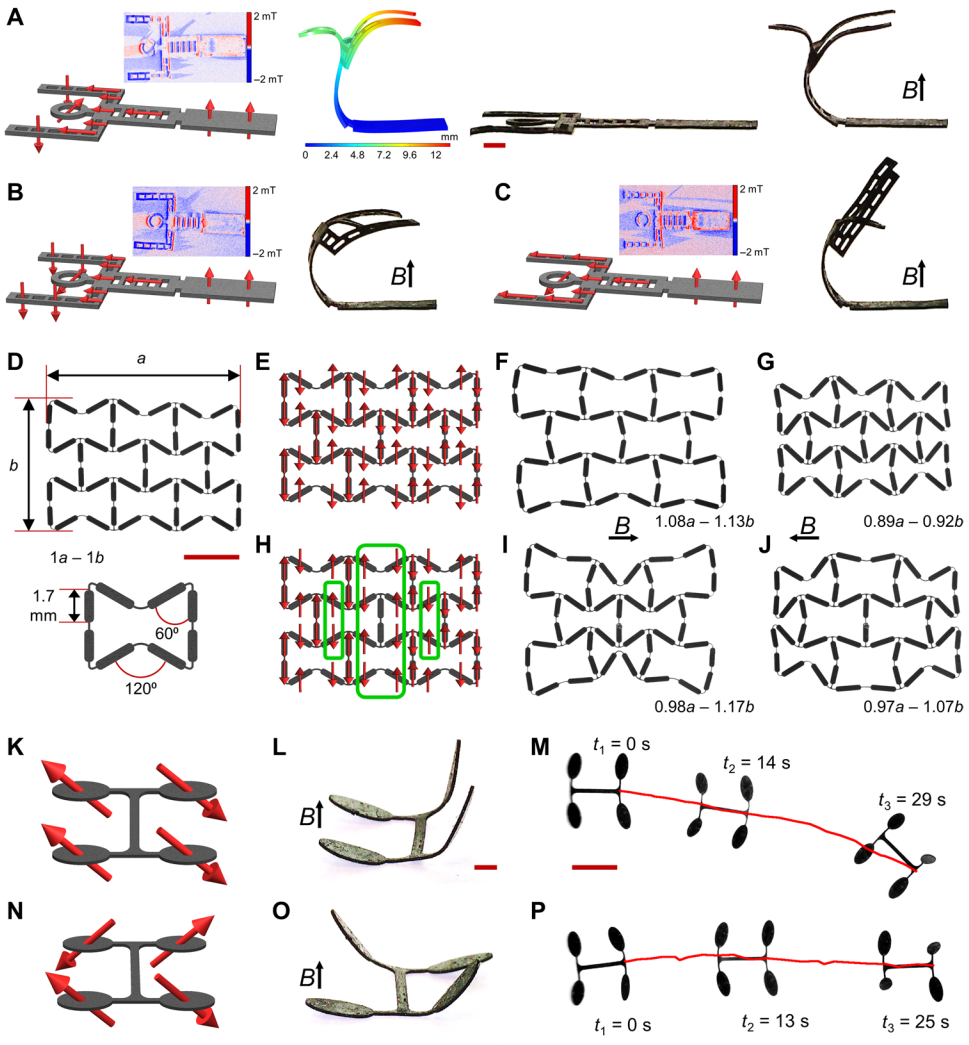


Fig. 3. Reprogrammable magnetization of 2D magnetic soft machines. (**A**) Distributed 3D magnetizations, out-of-plane magnetic flux density profile measurements, finite element simulations, and experimental shape changes upon magnetic actuation of a stickman structure. (**B** and **C**) Reprogramming the distributed magnetization directions in the stickman structure enables reconfiguring the shape changes. Red arrows indicate local magnetization directions. Color bars indicate magnetic flux density strength and total deformation, respectively. Scale bar, 1 mm. (**D** to **J**) Tuning mechanical behavior of an auxetic metamaterial by reprogramming the distributed magnetization profile of individual units. The length and width of the whole structure are denoted with *a* and *b*, respectively. (**E** to **G**) The flexible auxetic structure expands and compresses both in length and width depending on the magnetic actuation direction, displaying a negative Poisson's ratio. (**H** to **J**) Reprogramming the magnetization profile of three units in the middle results in an expansion in width with minimal change in length irrespective of the magnetic actuation direction. Red arrows indicate local magnetization directions. Green solid lines show the reprogrammed regions. Scale bar, 5 mm. Actuation of the structures is performed by applying uniform magnetic fields of 60 mT in the directions indicated with the black arrows. (**K** to **P**) Reprogramming magnetization profile of a quadrupedal soft robot enables tunable locomotion patterns. (K and N) Magnetization directions of the legs are programmed to generate different deformation configurations. Red arrows indicate local magnetization directions. (L and O) Upon magnetic actuation (20 mT) indicated with the black arrows, the legs deform in accordance with their magnetization directions. Scale bar, 1 mm. (M and P) Flexible robots with different magnetization profiles generate different locomotion patterns with rotational magnetic actuation. Scale bar, 5 mm.

present a 3D-printed nonmagnetic tree body with 2D magnetic leaves assembled at the tips of branches (movie S2). Magnetization direction of a leaf is programmed by laser-based heating while applying a magnetic field in a desired direction, which results in deformation of only the programmed leaf upon magnetic actuation (Fig. 4B). Sequential programming of all magnetic leaves in the same direction results in actuation of all leaves synchronously in the same direction (Fig. 4C). Furthermore, the magnetization direction of individual leaves can be reprogrammed on-demand to generate different configurations (Fig. 4D; fig. S5, K and L; and movie S2), enabling control over shape deformation instructions of 2D structures arranged in 3D configurations. Magnetic reprogramming of these 3D configurations can enable the development of reconfigurable soft machines for adaptive interaction with objects of arbitrary morphologies. As an example, we build an adaptive soft gripper composed of four fingers made from magnetic soft elastomers (Fig. 4E). Out-of-plane magnetization of fingers results in maximum deflection at the fingertips and enables squeezing of a spherical object (3-mm diameter) below the circumference (Fig. 4F and movie S2). On the other hand, a vertically placed cylindrical object (4-mm

Downloaded from http://advances.sciencemag.org/ on November 19, 2020

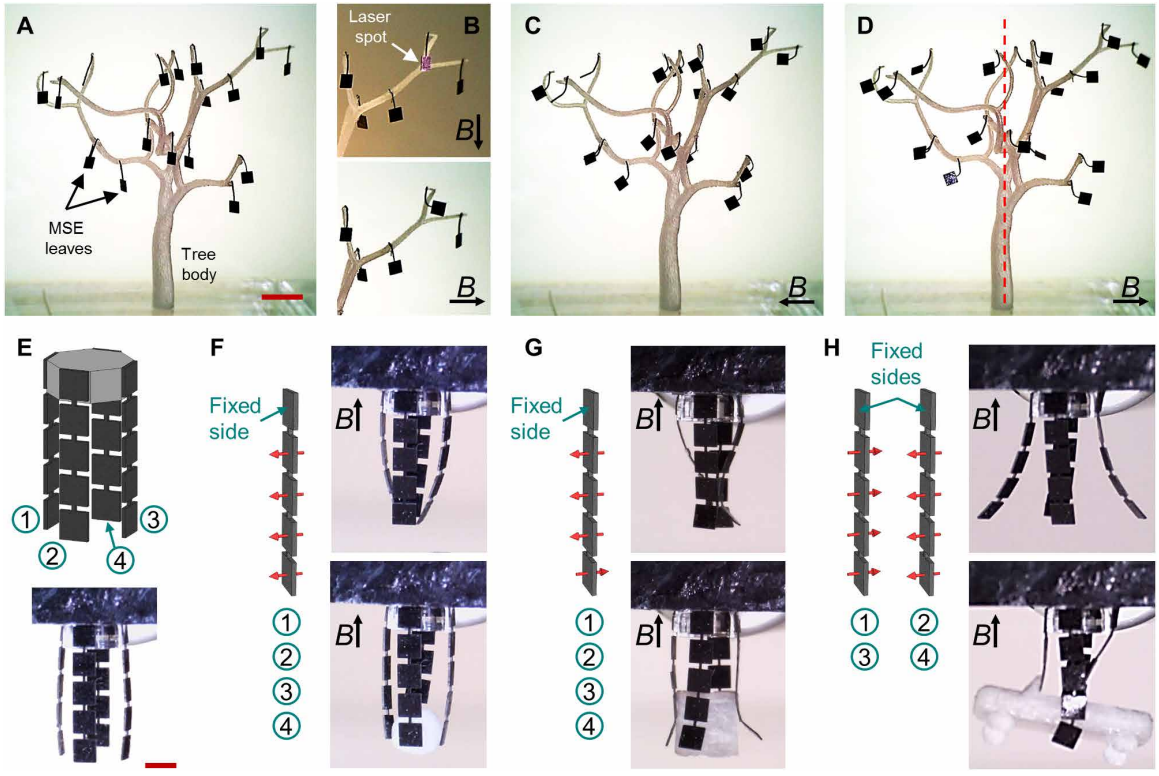


Fig. 4. Reprogrammable magnetization of 3D-configured magnetic soft machines. (**A** to **D**) Reprogrammable magnetization of flexible 2D magnetic leaves distributed on a 3D-printed nonmagnetic body. (B and C) Magnetization direction of individual leaves is programmed by local laser heating. (D) Magnetization direction of half of the leaves, indicated by the red dashed line, is reprogrammed in the reverse direction. Scale bar, 5 mm. (**E** to **H**) A four-finger adaptive soft gripper, enabled by reprogramming magnetization profile of the fingers. (F to H) Shape deformation of the fingers is reprogrammed to grasp objects with different morphologies, including a sphere (3-mm diameter) (F), a rod (4-mm diameter and 4-mm height) (G), and a car representing complex morphology (10.6-mm length, 3-mm width, and 1.75-mm height) (H). Red arrows indicate local magnetization directions. Scale bar, 2 mm. Actuation of the structures is performed by applying uniform magnetic fields of 60 mT in the directions indicated with the black arrows.

diameter and 4-mm height) requires a larger contact area with the gripping fingers, which is achieved by concave deflection of the fingers via magnetization profile as shown in Fig. 4G. Grasping a more complex example of a car-like object (10.6-mm length, 3-mm width, and 1.75-mm height), with an inner cavity and a gap underneath due to the wheels, is achieved by outward deformation of fingers within the inner cavity and inward deformation of the fingers at the sides (Fig. 4H and movie S2). Compared with existing approaches (*6*, *7*, *10*, *11*, *13*), our laser-based heat-assisted magnetization strategy enables on-demand and local reprogramming of 2D magnetic soft structures in 3D configurations with arbitrary magnetization profiles.

Microscale robots and machines hold remarkable potential for manipulation of the microscopic world with applications ranging from bioengineering to minimally invasive medicine (*24*–*27*). Magnetically programmed shape deformations can enable a new class of microsystems with advanced locomotion and manipulation capabilities. Our heat-assisted magnetization approach can be scaled down to program microstructures with a spatial resolution of 38 μm (Fig. 5). One route for down-scaling is focusing the NIR laser beam size below 200 μm by using a microscope objective (Fig. 5A). Using focused laser heating, a soft structure with six petals (150-μm width, 500-μm length, and 30-μm thickness) is magnetized in complimentary directions to generate synchronized deformation of petals in reverse directions (Fig. 5, B and C, and movie S3). Microscale magnetic programming can also be achieved by placing a photomask on top of the magnetic soft elastomers (Fig. 5, D to F). Photomask allows laser to pass through the micropatterned areas of different sizes, with the smallest dimension of 65 μm (fig. S10A), thus decreasing the area of the heated region to the patterned area. Using photomask-enabled micropatterned laser heating, "MPI" letters are magnetically programmed in different sizes and magnetization directions in magnetic soft elastomers, as shown by measured magnetic flux density profile (Fig. 5, E and F).

Other than laser-based sequential heating and magnetization, magnetic programming can also be realized by generating the desired magnetic pattern (master) in close proximity to the magnetic soft elastomers (slave) and heating the system globally (Fig. 5G), enabling one-shot magnetization of the whole sample. For creating magnetic masters, polyurethane neodymium-iron-boron (NdFeB) composite magnets, with a higher Curie temperature than CrO_2, of different sizes, shapes, and polarities in different configurations are manually arranged (Fig. 5, H and I). Magnetic one-shot pattern transfer is achieved by putting the magnetic soft elastomer slaves in direct contact with the magnetic masters and globally heating to 150°C (Fig. 5, H and I). We further fabricate a magnetic master with a complex "Minerva" symbol (Fig. 5J and fig. S10B). By contact magnetic transfer, magnetic profile of the magnetic master is copied into

Downloaded from http://advances.sciencemag.org/ on November 19, 2020

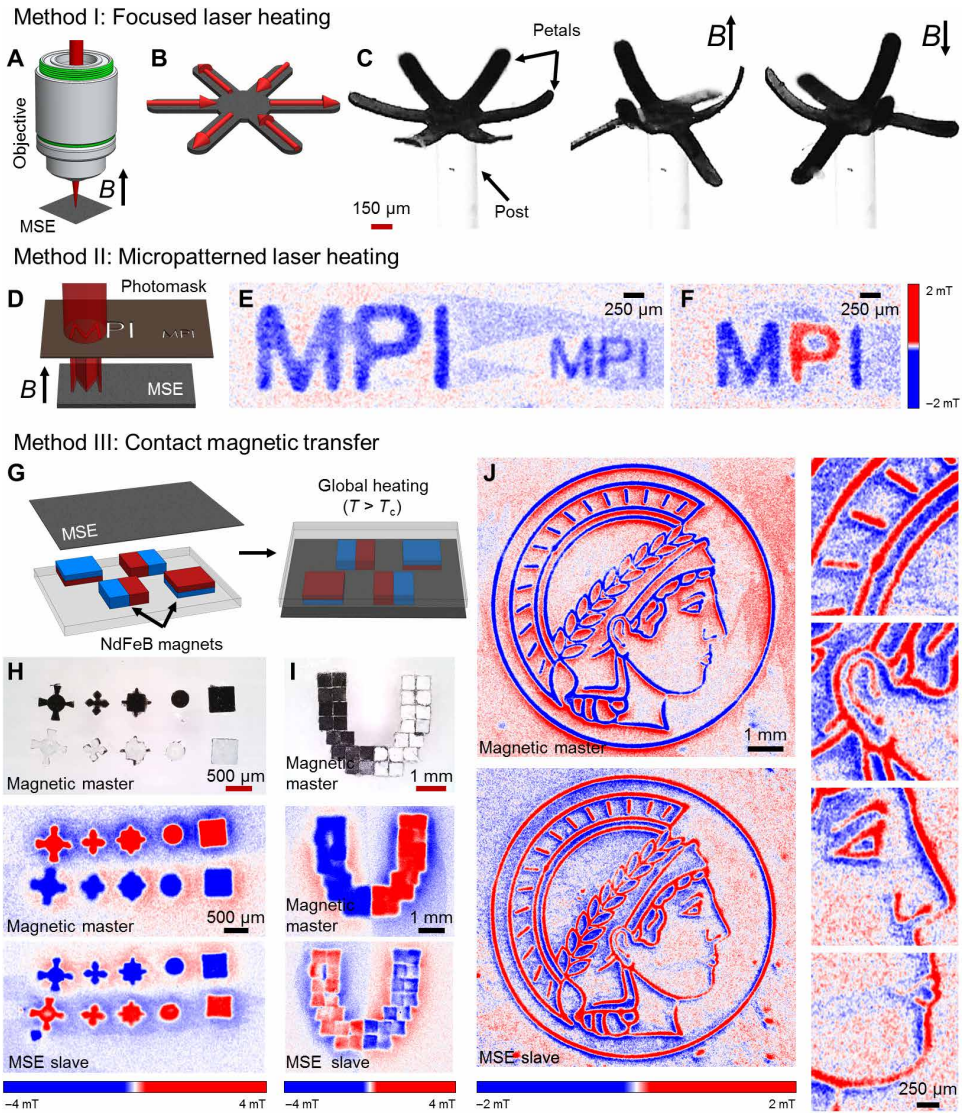


Fig. 5. Heat-assisted magnetic programming of soft materials at the microscale. (**A**) Scanning a focused laser spot on a magnetic soft elastomer (MSE), which creates a precisely controlled local heating, in a desired pattern is used to program the magnetization profile on that material. (**B** and **C**) An example soft structure with six petals (150-μm width, 500-μm length, and 30-μm thickness) is placed on a micropost. Red arrows indicate the magnetization directions of the petals. Magnetic actuation (60 mT) resulted in deformation of petals in reverse directions. (**D**) A collimated laser can heat a desired shape on a target magnetic soft elastomer in one shot through a mask containing the micropattern of this desired shape. (**E** and **F**) Magnetic flux density measurements of example magnetically programmed samples by this micropatterned laser heating. The smallest magnetic pattern is 80 μm in width. Scale bars, 250 μm. (**G**) Contact transfer of desired magnetic profiles in one shot via global heating. The magnetic soft elastomer is placed in direct contact with NdFeB magnets, with a greater Curie temperature, arranged in different configurations and heated above the Curie temperature of the CrO_2. Magnetization directions of the NdFeB magnets are transferred to the magnetic soft elastomer during cooling. (**H** and **I**) Magnetic flux density measurements of the NdFeB masters of different example shapes and configurations and the magnetic soft elastomer slaves. Scale bars, 500 μm and 1 mm, respectively. (**J**) Contact transfer of a complex magnetization profile in the geometric pattern of Minerva. Insets show close up views of the magnetic flux density profile of the magnetic soft elastomer slave. The smallest magnetic pattern is 38 μm in width. Color bars indicate magnetic flux density strength. Scale bars, 1 mm and 250 μm, respectively.

a magnetic soft elastomer slave, with the smallest dimension of 38 μm (Fig. 5J). While high-resolution 2D magnetic programming has been previously shown in rigid panels connected via flexible hinges (*10*), heat-assisted magnetization strategy described here enables 3D magnetic programming at a comparable resolution (fig. S6). Moreover, heat-assisted magnetic contact transfer shown in Fig. 4 (G to J) can be adapted for high-throughput magnetic encoding using a magnetic master and a three-axis stage, which enables programming 10 samples/min using a single master (movie S4).

DISCUSSION

Heat-assisted magnetic programming strategy introduced here is inherently decoupled from the fabrication method of the magnetic soft elastomers and enables a noninvasive mean for reprogramming shape deformations at high spatial resolutions. Discrete and 3D magnetization is shown for development of a variety of magnetic soft machines from undulating swimmers and crawlers to multi-armed grippers and magnetic mirror mounts (*7*). In situ magnetic reprogrammability, on top of 3D and discrete magnetization, introduced

Downloaded from http://advances.sciencemag.org/ on November 19, 2020

here enables reconfigurable soft machines that can interact with unstructured surroundings and arbitrary objects in an adaptive manner, such as the gripper demonstration shown in Fig. 4 (E to H). We have further shown that local magnetic reprogramming allows facile reconfiguration of mechanical metamaterials, thus their internal material behavior. 3D magnetic metamaterials with bidirectionally programmed domains are proposed and shown to undergo complex shape changes under external magnetic fields (*13*). 3D magnetic reprogramming capability enabled by our approach can further enable rapid and data-based optimization of performance and behavior of soft mechanical and optical metamaterials and kirigami-enabled structures.

Magnetic programming at the microscale could enable the development of microrobots with complex locomotion capabilities. Previous work has demonstrated 2D magnetic programming on rigid square micro panels (10 μm by 10 μm) interconnected with hinges (*10*). While the maximum resolution demonstrated in our work is ~38 μm, 3D magnetization capability along with (re)programming inherently soft materials could enable more complex deformations and, thus, the development of bioinspired microrobots. Moreover, resolution and speed of heat-assisted magnetic programming can be further scaled down using well-established magneto-optical recording techniques used in the data storage industry (*28*, *29*). High-throughput magnetic contact transfer could also be combined with multiple masters of desired magnetic profiles and mechanical punchers to cut the magnetic soft elastomer samples in desired shapes, paving the way for future continuous roll-to-roll mass production of magnetic soft machines (fig. S6).

While the laser heating-based magnetization approach presented here allows (re)programming of magnetic 2D sheets, penetration depth of the laser heating limits the addressable thickness of the magnetic elastomer. Although our approach enables magnetic programming of 2D structures arranged in 3D configurations, limited penetration depth of the laser heating also prevents magnetic (re)programming of intrinsically 3D structures. Laser-based heating is also not feasible for (re)programming of magnetic soft machines inside the human body. However, we would still use our discrete and 3D magnetization approach for high-resolution and high-throughput programming (not reprogramming) of magnetic soft robots and devices in future minimally invasive medicine applications. Furthermore, remote and selective heating can also be achieved by remote power transfer to thin receiver coils attached onto the elastomers (*30*). Remote magnetic (re)programming can enable adaptive operation of soft untethered machines in closed and confined dynamic environments. Magnetically responsive multiscale soft machines with reprogrammable complex shape transformation capabilities will inspire diverse applications in medical robots, wearable health monitoring devices, and bio-inspired microrobots.

MATERIALS AND METHODS

Preparation of magnetic elastomers

CrO_2 powder (Sigma-Aldrich, St. Louis, MO) was pretreated with sodium bisulfite to create a stabilized form with a reduced barrier surface layer, preventing reactions with water and organic materials (*22*, *31*). First, the powder was heated for 3 hours at 300°C. Twenty-two grams of baked CrO_2 particles were dispersed in 250 ml of sodium bisulfite solution in deionized (DI) water (50 g/liter; Sigma-Aldrich, St. Louis, MO) and kept at 65°C for 16 hours while agitated occasionally. Then, the particles were washed five times with DI water and filtered by using a test sieve with a mesh size of 20 μm. The remaining CrO_2 particles were left in a fume hood for 2 days to remove any remaining water. The resulting film was scraped and crushed using a pestle and mortar to obtain final dried and stabilized CrO_2 particles.

CrO_2/PDMS magnetic soft elastomer composites were prepared by adding the dried and stabilized CrO_2 particles into the siloxane base (Dow Corning, Midland, MI) at 1:2 (CrO_2:siloxane base) mass ratio and mixing for 5 min. Next, the cross-linking agent was added into the prepolymer mixture at a cross-linking agent to mixture mass ratio of 1:10 and further mixed. Then, the mixture was cast into molds composed of high temperature–resistant tapes (Kapton polyimide films, DuPont, Wilmington, DE) of desired thicknesses adhered on a flat glass substrate and cured for 4 hours at 90°C. An ultraviolet laser system (LPKF ProtoLaser U3, Garbsen, Germany) was used to cut the desired geometries out of the magnetic elastomer films. The thickness of the magnetic elastomer films was measured with an optical profilometer (VK-X250, Keyence, Osaka, Japan). Elastic modulus (E) and strain of the magnetic elastomers at break were experimentally characterized by uniaxial tensile testing of nonheated and heated dog bone–shaped samples at a strain rate of 0.005 s^{-1} (Instron 5942, Instron, Norwood, MA).

Heat-assisted magnetic (re)programming

Local heating of CrO_2 elastomer films was achieved by using a power-adjustable fiber-coupled NIR laser with a collimator (808 nm, 133 to 457 mW; Edmund Optics, Barrington, NJ). The temperature and the heated spot size on the magnetic elastomer films were measured using an infrared thermal camera (ETS320, Wilsonville, OR) at a distance of 7 cm. Heating and cooling times of the magnetic soft elastomers were measured by heating the samples for 100 s. Samples were placed on an automated stage (Axidraw v3, Evil Mad Scientist, Sunnyvale, CA) and NdFeB magnet (20-mm diameter and 20-mm thickness; Supermagnete, Gottmadingen, Germany) that can be rotated 360° were placed underneath the magnetic soft elastomer at a distance of 20.4 mm during heating and cooling to align the magnetization direction of the CrO_2 particles (fig. S8, A and B, and movie S4). The arrangement of the magnet and sample locations ensured generation of sufficient and uniform magnetic field on both top and bottom sides of the laser-heated area (fig. S9). Applied magnetic field magnitude and direction were continuously monitored by using a 3D magnetic Hall effect sensor (TLE493D-W2B6, Infineon Technologies, Munich, Germany) and adjusted according to the desired magnetization direction.

Magnetization of the magnetic soft elastomers was measured with a vibrating sample magnetometer (VSM; MicroSense, Lowell, MA). Circular samples with a diameter of 1 mm were placed on a sample holder, and hysteresis loop of CrO_2 was obtained at external fields ranging from 1.5 to −1.5 T (fig. S1A). Magnetization of the magnetic soft elastomers was calculated as 9.8 kA/m, by dividing the remanent magnetization to the sample volume. Magnetization efficiency was determined as the ratio of magnetization of the heat-magnetized samples and samples magnetized under 1.8-T field in VSM. Magnetization profile of the magnetically programmed samples was characterized by measuring the magnetic flux densities at sample surfaces via a magneto-optical sensor (fig. S1D; MagViewS, Matesy, Jena, Germany).

Downloaded from http://advances.sciencemag.org/ on November 19, 2020

Computational modeling of shape deformations

Finite element analysis is used for predictive modeling of the shape changes under magnetic actuation (fig. S7). COMSOL structural mechanics module (COMSOL, Burlington, MA) is linked to a custom MATLAB script (MathWorks, Natick, MA) via "LiveLink." Sample geometries are divided into smaller subsections with predefined magnetization profiles, and MATLAB script is used for calculation of magnetic forces and torques, while mechanical deformations are solved in COMSOL. After every iteration, magnetic forces and torques were recalculated according to the updated magnetization direction vector for each subsection until a quasistatic equilibrium state in 3D is reached. For all simulations, experimentally measured E of 200 kPa and magnetization of 9.8 kA/m were used. The density of the magnetic soft elastomer was calculated as 1.318 g/cm^3, and the Poisson's ratio is assumed to be 0.49.

Magnetic actuation

A cylindrical NdFeB magnet (60-mm diameter and 10-mm thickness; Supermagnete, Gottmadingen, Germany) was approached to the samples in the vertical or horizontal direction for magnetic actuation (fig. S8C). For magnetic actuation under uniform fields, a Halbach array composed of 16 permanent magnets (10 mm by 10 mm by 10 mm) was used (fig. S8D). The magnet was rotated underneath the sample for the rotational actuation. Actuation videos were recorded using a benchtop digital microscope (Dino-Lite AM7013MZT, AnMo Electronics, Hsinchu, Taiwan) at 10 fps.

Magnetic (re)programming at the micron scale

For magnetic (re)programming at the micron scale, three different approaches were used: focused laser heating, photomask-enabled micropatterned laser heating, and contact magnetic transfer via global heating. Focused laser heating was achieved by placing a microscope objective (20×, 0.5 numerical aperture; Carl Zeiss, Oberkochen, Germany) in the laser beam path and decreasing the beam size below 200 μm. For photomask-enabled micropatterned laser heating, a photomask containing microscale patterns (fig. S10A) was placed on top of the samples with a 20-μm gap. When exposed to the laser beam, which can only pass through the micropatterned areas, the samples were heated locally in the shape of patterns available on the photomask. For contact transfer of magnetic profiles, polyurethane NdFeB magnetic composites of different shapes were used. First, an SU-8 positive template of desired geometries (fig. S10B) on a silicon wafer was fabricated by photolithography and wet chemical development. Then, a silicone rubber (Mold Max 20, Smooth-On, Macungie, PA) was poured over the positive template, cured at room temperature for 4 hours, and peeled off, resulting in a negative template. Afterward, polyurethane prepolymer (Smooth-Cast 310/1, Smooth-On, Macungie, PA) mixed with NdFeB powder (MQFP-15-7, Magnequench, Toronto, Canada) at 1:1 mass ratio was molded into the negative template and cured for 4 hours at room temperature and peeled off. Prepared polyurethane NdFeB magnets were premagnetized in VSM under a 1.8-T uniform magnetic field, and magnetic fields generated by polyurethane NdFeB magnets were smaller than the coercivity of the magnetic soft elastomers. While modular polyurethane magnets were manually arranged in desired configurations, the ones with complex shapes were used as monolithic units. Last, for contact magnetic transfer, the magnetic soft elastomer slaves were placed on top of polyurethane NdFeB masters and placed into an oven for 5 min at 150°C and cooled down to room temperature while in contact. The maximum thickness of the slave that can be effectively magnetized in perpendicular direction using a 200-μm-thick master with a 50% magnetic particle mass ratio is around 180 μm (fig. S11). However, the effective thickness of the slave can be increased with carefully designed magnetic masters for the desired magnetization profiles (fig. S11).

SUPPLEMENTARY MATERIALS

Supplementary material for this article is available at http://advances.sciencemag.org/cgi/content/full/6/38/eabc6414/DC1

REFERENCES AND NOTES

1. Y. Kim, G. A. Parada, S. Liu, X. Zhao, Ferromagnetic soft continuum robots. *Sci. Robot.* **4**, eaax7329 (2019).
2. M. Cianchetti, C. Laschi, A. Menciassi, P. Dario, Biomedical applications of soft robotics. *Nat. Rev. Mater.* **3**, 143–153 (2018).
3. M. Sitti, Miniature soft robots — Road to the clinic. *Nat. Rev. Mater.* **3**, 74–75 (2018).
4. E. T. Roche, M. A. Horvath, I. Wamala, A. Alazmani, S.-E. Song, W. Whyte, Z. Machaidze, C. J. Payne, J. C. Weaver, G. Fishbein, J. Kuebler, N. V. Vasilyev, D. J. Mooney, F. A. Pigula, C. J. Walsh, Soft robotic sleeve supports heart function. *Sci. Transl. Med.* **9**, eaaf3925 (2017).
5. X. Yu, Z. Xie, Y. Yu, J. Lee, A. Vazquez-Guardado, H. Luan, J. Ruban, X. Ning, A. Akhtar, D. Li, B. Ji, Y. Liu, R. Sun, J. Cao, Q. Huo, Y. Zhong, C. M. Lee, S. Y. Kim, P. Gutruf, C. Zhang, Y. Xue, Q. Guo, A. Chempakasseril, P. Tian, W. Lu, J. Y. Jeong, Y. J. Yu, J. Cornman, C. S. Tan, B. H. Kim, K. H. Lee, X. Feng, Y. Huang, J. A. Rogers, Skin-integrated wireless haptic interfaces for virtual and augmented reality. *Nature* **575**, 473–479 (2019).
6. W. Hu, G. Z. Lum, M. Mastrangeli, M. Sitti, Small-scale soft-bodied robot with multimodal locomotion. *Nature* **554**, 81–85 (2018).
7. T. Xu, J. Zhang, M. Salehizadeh, O. Onaizah, E. Diller, Millimeter-scale flexible robots with programmable three-dimensional magnetization and motions. *Sci. Robot.* **4**, eaav4494 (2019).
8. M. J. Ford, C. P. Ambulo, T. A. Kent, E. J. Markvicka, C. Pan, J. Malen, T. H. Ware, C. Majidi, A multifunctional shape-morphing elastomer with liquid metal inclusions. *Proc. Natl. Acad. Sci. U.S.A.* **116**, 21438–21444 (2019).
9. J. A.-C. Liu, J. H. Gillen, S. R. Mishra, B. A. Evans, J. B. Tracy, Photothermally and magnetically controlled reconfiguration of polymer composites for soft robotics. *Sci. Adv.* **5**, eaaw2897 (2019).
10. J. Cui, T.-Y. Huang, Z. Luo, P. Testa, H. Gu, X.-Z. Chen, B. J. Nelson, L. J. Heyderman, Nanomagnetic encoding of shape-morphing micromachines. *Nature* **575**, 164–168 (2019).
11. J. Kim, S. E. Chung, S.-E. Choi, H. Lee, J. Kim, S. Kwon, Programming magnetic anisotropy in polymeric microactuators. *Nat. Mater.* **10**, 747–752 (2011).
12. S. Fusco, M. S. Sakar, S. Kennedy, C. Peters, R. Bottani, F. Starsich, A. Mao, G. A. Sotiriou, S. Pané, S. E. Pratsinis, D. Mooney, B. J. Nelson, An integrated microrobotic platform for on-demand, targeted therapeutic interventions. *Adv. Mater.* **26**, 952–957 (2014).
13. Y. Kim, H. Yuk, R. Zhao, S. A. Chester, X. Zhao, Printing ferromagnetic domains for untethered fast-transforming soft materials. *Nature* **558**, 274–279 (2018).
14. Z. Ren, W. Hu, X. Dong, M. Sitti, Multi-functional soft-bodied jellyfish-like swimming. *Nat. Commun.* **10**, 2703 (2019).
15. J. J. Abbott, E. Diller, A. J. Petruska, Magnetic methods in robotics. *Annu. Rev. Control, Robot. Auton. Syst.* **3**, 57–90 (2020).
16. M. Sitti, *Mobile Microrobotics* (MIT Press, 2017).
17. R. M. Erb, J. J. Martin, R. Soheilian, C. Pan, J. R. Barber, Actuating soft matter with magnetic torque. *Adv. Funct. Mater.* **26**, 3859–3880 (2016).
18. G. Z. Lum, Z. Ye, X. Dong, H. Marvi, O. Erin, W. Hu, M. Sitti, Shape-programmable magnetic soft matter. *Proc. Natl. Acad. Sci. U.S.A.* **113**, E6007–E6015 (2016).
19. Q. Ze, X. Kuang, S. Wu, J. Wong, S. M. Montgomery, R. Zhang, J. M. Kovitz, F. Yang, H. J. Qi, R. Zhao, Magnetic shape memory polymers with integrated multifunctional shape manipulation. *Adv. Mater.* **32**, 1906657 (2020).
20. M. M. Schmauch, S. R. Mishra, B. A. Evans, O. D. Velev, J. B. Tracy, Chained iron microparticles for directionally controlled actuation of soft robots. *ACS Appl. Mater. Interfaces* **9**, 11895–11901 (2017).
21. H.-W. Huang, M. S. Sakar, A. J. Petruska, S. Pané, B. J. Nelson, Soft micromachines with programmable motility and morphology. *Nat. Commun.* **7**, 12263 (2016).
22. M. Li, Y. Wang, A. Chen, A. Naidu, B. S. Napier, W. Li, C. L. Rodriguez, S. A. Crooker, F. G. Omenetto, Flexible magnetic composites for light-controlled actuation and interfaces. *Proc. Natl. Acad. Sci. U.S.A.* **115**, 8119–8124 (2018).
23. M. Liu, J. Sun, Q. Chen, Influences of heating temperature on mechanical properties of polydimethylsiloxane. *Sens. Actuators A Phys.* **151**, 42–45 (2009).

Downloaded from http://advances.sciencemag.org/ on November 19, 2020

24. Y. Alapan, B. Yigit, O. Beker, A. F. Demirörs, M. Sitti, Shape-encoded dynamic assembly of mobile micromachines. *Nat. Mater.* **18**, 1244–1251 (2019).
25. Y. Alapan, O. Yasa, O. Schauer, J. Giltinan, A. F. Tabak, V. Sourjik, M. Sitti, Soft erythrocyte-based bacterial microswimmers for cargo delivery. *Sci. Robot.* **3**, eaar4423 (2018).
26. Y. Alapan, O. Yasa, B. Yigit, I. C. Yasa, P. Erkoc, M. Sitti, Microrobotics and microorganisms: Biohybrid autonomous cellular robots. *Annu. Rev. Control Robot. Auton. Syst.* **2**, 205–230 (2019).
27. Y. Alapan, U. Bozuyuk, P. Erkoc, A. C. Karacakol, M. Sitti, Multifunctional surface microrollers for targeted cargo delivery in physiological blood flow. *Sci. Robot.* **5**, eaba5726 (2020).
28. M. H. Kryder, Magneto-optic recording technology. *J. Appl. Phys.* **57**, 3913–3918 (1985).
29. W. A. Challener, C. Peng, A. V. Itagi, D. Karns, W. Peng, Y. Peng, X. M. Yang, X. Zhu, N. J. Gokemeijer, Y.-T. Hsia, G. Ju, R. E. Rottmayer, M. A. Seigler, E. C. Gage, Heat-assisted magnetic recording by a near-field transducer with efficient optical energy transfer. *Nat. Photon.* **3**, 220–224 (2009).
30. M. Boyvat, J.-S. Koh, R. J. Wood, Addressable wireless actuation for multijoint folding robots and devices. *Sci. Robot.* **2**, eaan1544 (2017).
31. W. G. Bottjer, H. G. Ingersoll, Stabilized ferromagnetic chromium dioxide. US Patent 3512930 (1970).

Acknowledgments: We thank B. Yigit for initial discussions, V. Sridhar for helping with the pretreatment of chromium dioxide powder, N. Krishna-Subbaiah and X. Dong for helping with the microfabrication of polyurethane molds, O. Cakici for helping with the laser heating setup, M. C. Ugurlu and D. Son for the Halbach array setup, M. Yunusa for helping with the tensile testing measurements, and O. Yasa for helping with the magnetic characterizations. **Funding:** Y.A. thanks the Alexander von Humboldt Foundation for the Humboldt Postdoctoral Research Fellowship. This work was funded by the Max Planck Society and European Research Council (ERC) Advanced Grant SoMMoR project with grant no. 834531. **Author contributions:** Y.A. and A.C.K. participated in the study design, experimental procedures, data collection, data analysis, and manuscript writing. S.N.G. and I.I. assisted with the experimental procedures, data collection, and data analysis. M.S. participated in the study design, research supervision, and manuscript writing. **Competing interests:** Y.A., A.C.K., and M.S. are inventors on a patent application EP20171719.6 submitted by the Max Planck Innovation GmbH. S.N.G. and I.I. declare that they have no competing interests. **Data and materials availability:** All data needed to evaluate the conclusions in the paper are present in the paper and/or the Supplementary Materials. Additional data related to this paper may be requested from the authors.

Submitted 5 May 2020
Accepted 31 July 2020
Published 18 September 2020
10.1126/sciadv.abc6414

Citation: Y. Alapan, A. C. Karacakol, S. N. Guzelhan, I. Isik, M. Sitti, Reprogrammable shape morphing of magnetic soft machines. *Sci. Adv.* **6**, eabc6414 (2020).

Downloaded from http://advances.sciencemag.org/ on November 19, 2020

Science Advances

Reprogrammable shape morphing of magnetic soft machines

Yunus Alapan, Alp C. Karacakol, Seyda N. Guzelhan, Irem Isik and Metin Sitti

Sci Adv **6** (38), eabc6414.
DOI: 10.1126/sciadv.abc6414

ARTICLE TOOLS http://advances.sciencemag.org/content/6/38/eabc6414

SUPPLEMENTARY MATERIALS http://advances.sciencemag.org/content/suppl/2020/09/14/6.38.eabc6414.DC1

REFERENCES This article cites 29 articles, 5 of which you can access for free
http://advances.sciencemag.org/content/6/38/eabc6414#BIBL

PERMISSIONS http://www.sciencemag.org/help/reprints-and-permissions

Use of this article is subject to the Terms of Service

Science Advances (ISSN 2375-2548) is published by the American Association for the Advancement of Science, 1200 New York Avenue NW, Washington, DC 20005. The title *Science Advances* is a registered trademark of AAAS.

Copyright © 2020 The Authors, some rights reserved; exclusive licensee American Association for the Advancement of Science. No claim to original U.S. Government Works. Distributed under a Creative Commons Attribution NonCommercial License 4.0 (CC BY-NC).

Downloaded from http://advances.sciencemag.org/ on November 19, 2020